

Modeling of the $X\ ^1\Sigma^+, a\ ^3\Sigma^+ \rightarrow E(4)\ ^1\Sigma^+ \rightarrow X\ ^1\Sigma^+(v=0, J=0)$ optical cycle for ultracold KCs molecule production

I. Klincare, O. Nikolayeva, M. Tamanis, and R. Ferber*

Laser Center, Department of Physics, University of Latvia, 19 Rainis Boulevard, Riga LV-1586, Latvia

E. A. Pazyuk and A. V. Stolyarov†

Department of Chemistry, Moscow State University, 119991, GSP-2, Moscow, Leninskie gory 1/3, Russia

(Received 10 May 2012; published 28 June 2012)

We present experimental relative intensity distribution and theoretical radiative probabilities for the spin-allowed $E(4)\ ^1\Sigma^+ - X\ ^1\Sigma^+$ and spin-forbidden $E(4)\ ^1\Sigma^+ - a\ ^3\Sigma^+$ rovibronic transitions studied in the KCs molecule. The absorption and emission Einstein coefficients were predicted in a wide range of vibrational v and rotational J quantum numbers for both singlet-singlet $E - X$ and singlet-triplet $E - a$ rovibronic transitions along with radiative lifetimes of the upper E state and branching ratios of spontaneous emission into the lower-lying electronic states, including both bound-bound and bound-continuum parts of the spectra. The required spin-allowed $E(4)\ ^1\Sigma^+ - X; A; C\ ^1\Sigma^+; B\ ^3\Pi$ transition dipole moments were obtained in the framework of quasirelativistic electronic structure calculations. The regular spin-orbit coupling with the nearest $^3\Pi$ states is found to be sufficient to induce the spin-forbidden $E(4)\ ^1\Sigma^+ - a; c\ ^3\Sigma^+; b\ ^3\Pi$ transitions by borrowing probabilities from the relevant $(1-5)\ ^3\Pi - (a; c)\ ^3\Sigma^+; b\ ^3\Pi$ transitions. Relative intensity distributions in rotationally resolved $E \rightarrow X$ and $E \rightarrow a$ laser-induced fluorescence (LIF) progressions were determined from Fourier transform spectra. Experimental LIF intensity distributions demonstrated good agreement with their predicted counterparts. The simulations demonstrate that the translationally ultracold KCs molecules could be efficiently produced in their absolute ground state in one stimulated Raman step $X\ ^1\Sigma^+; a\ ^3\Sigma^+(v'') \rightarrow E(4)\ ^1\Sigma^+(v'_E = 44, J'_E = 1) \rightarrow X\ ^1\Sigma^+(v''_X = 0, J''_X = 0)$ from the weakly bound rovibronic levels v'' of both singlet X and triplet a states.

DOI: [10.1103/PhysRevA.85.062520](https://doi.org/10.1103/PhysRevA.85.062520)

PACS number(s): 33.70.Ca, 37.10.Mn, 33.20.Wr

I. INTRODUCTION

Cold and ultracold samples of polar diatomic molecules continue to be a hot topic of research, offering a number of applications. Because of dominating long-range dipolar interactions that can be guided by external electric field, such species are expected to be exemplary for controlled ultracold chemistry, quantum many-body physics (quantum magnetism and quantum phases, quantum computing), high-precision metrology, and tests of fundamental models (see [1,2] for a review). More recently, particular attention had been focused on deeply bound ground-state polar diatomics, aimed to produce them in the lowest rovibrational state with zero vibrational and rotational quantum numbers $v''_X = 0, J''_X = 0$, or $X(0,0)$ for short. Such samples are most attractive for potential applications because they are stable to inelastic collisions (except barrierless reaction) and possess larger electric dipole moments.

In a number of cases successful experiments have been carried out on diatomic molecules of heteronuclear alkali-metal atoms by applying photoassociation (PA) or magnetoassociation (MA) via Feshbach resonances applied to a high-density sample of the respective ultracold atoms. To transfer the initially very loosely bound translationally cold diatomic molecules to their deeply bound ground state, the two-photon scheme is most often used. In particular,

cold $^{40}\text{K}^{87}\text{Rb}$ species have been efficiently produced using stimulated Raman adiabatic passage (STIRAP) for transferring Feshbach molecules to the $X(0,0)$ state in [3]. Regarding Cs-containing alkali-metal dimers, cold LiCs $X(0,0)$ molecules were obtained in [4] using a single PA step followed by spontaneous emission, while NaCs molecules in deeply bound v''_X states were produced by near-dissociation PA in [5]. The authors of Ref. [6] produced RbCs molecules in $X(v=0, J)$ states using PA followed by an incoherent pump-dump cycle. The authors of Refs. [7,8] are planning to produce ultracold RbCs $X(0,0)$ species by applying STIRAP strategy.

To facilitate this task, it appeared important to identify suitable pathways $(X; a)\ ^1,^3\Sigma^+(v'', J'') \rightarrow X\ ^1\Sigma^+(0,0)$ that would allow efficient passage from weakly bound v'', J'' levels to the strongly bonded ones, including the lowest $X(0,0)$ levels (see Fig. 1 for an idea). Usually it means searching for a strongly mixed singlet-triplet intermediate upper rovibronic state, which could be excited by suitable lasers from high vibrational levels of the ground singlet $X\ ^1\Sigma^+$ and triplet $a\ ^3\Sigma^+$ states, at the same time having considerable probabilities to radiate to the absolute ground $X(0,0)$ state. Different intermediate states with the significantly mixed singlet-triplet character have been exploited for alkali-metal diatomics, such as the $A\ ^1\Sigma^+ \sim b\ ^3\Pi$ complex for RbCs [7], the $B\ ^1\Pi \sim c\ ^3\Sigma^+ \sim b\ ^3\Pi$ complex for RbCs [6,10], and for KRb [11].

In the present study we suggest to use for this purpose, in the case of KCs and presumably also of RbCs, a shelflike singlet $E(4)\ ^1\Sigma^+$ state (E state for short), which is regularly perturbed by a pronounced spin-orbit coupling (SOC) interaction with

*ferber@latnet.lv

†avstol@phys.chem.msu.ru

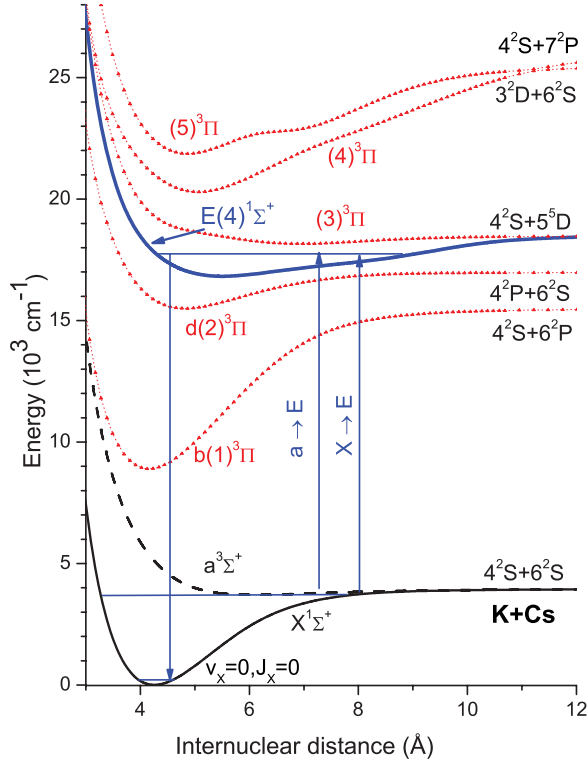


FIG. 1. (Color online) Schema of the initial $X^1\Sigma^+$; $a^3\Sigma^+$ and intermediate shelflike $E(4)^1\Sigma^+$ states of KCs involved in the two-step optical cycle, along with the (1–5) $^3\Pi$ states manifold, which regularly perturbs the E state due to pronounced spin-orbit coupling interaction. Vertical arrows denote pumping ($X \rightarrow E$, $a \rightarrow E$) and dumping ($E \rightarrow X$) stimulated transitions. The relevant nonrelativistic *ab initio* PECs are borrowed from Ref. [9]

the “surrounding” triplet $^3\Pi$ states (see Fig. 1). Here, E refers to an excited singlet state, while (4) is the ordinal number of a $^1\Sigma^+$ state. The unique properties of the $E(4)^1\Sigma^+$ state, making it favorable to use as the intermediate one in a two-step $X^1\Sigma^+$; $a^3\Sigma^+ \rightarrow E(4)^1\Sigma^+ \rightarrow X^1\Sigma^+(v=0, J=0)$ optical cycle, are (i) good overlap (Franck-Condon factors) of the vibrational functions for the particular vibrational level v'_E of the E state (located in the shelf region) simultaneously with lowest and highest vibrational levels of the ground singlet X state; (ii) a regular SOC effect yielding considerable probabilities of the nominally spin-forbidden $E - a$ transitions.

For Cs-containing diatomics, the excited state in question is the lowest state, which is asymptotically converging to the Cs(5^2D) atom. It is, for instance, the $C(3)^1\Sigma^+$ state for LiCs and NaCs, while the $E(4)^1\Sigma^+$ state for KCs and RbCs. The shelflike character of these states caused by avoided crossing of ion-pair and valence adiabatic potential energy curves (PECs) is most pronounced for a light partner atom such as in LiCs, becoming the smoothest in RbCs. Spectroscopic studies of these states were performed in [12,13] for RbCs, in [14] for KCs, and in [15] for LiCs (see also a note in [16] for NaCs). As shown in [17] for RbCs and in [14,18,19] for KCs, the $E(4)^1\Sigma^+$ state is coupled by optical transitions to the triplet a state, as well as to high v'_X levels of the singlet X state close to the dissociation limit. At the same time, $E \rightarrow X$ transitions to deeply bound X state levels occur with

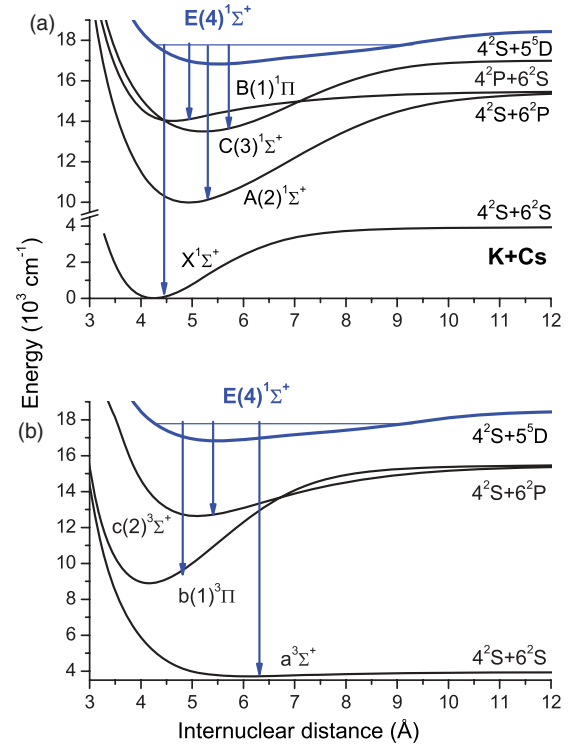


FIG. 2. (Color online) Schema of most pronounced decay channels of the KCs E state corresponding to (a) spin-allowed $E \rightarrow X; A; B; C$ and (b) spin-forbidden $E \rightarrow a; b; c$ transitions.

high-enough probability in laser-induced fluorescence (LIF) from a wide range of v'_E levels.

The goal of the present work is to model a two-step optical cycle suitable for producing deeply bound ultracold polar alkali-metal diatomics through an intermediate shelflike state. We focus on the KCs molecule, being the closest analog of RbCs due to vicinity of first resonant atomic transitions of Rb and K atoms. The data currently available in the literature for KCs are (i) highly accurate empirical PECs for both ground singlet X and triplet a states [18,19] as well as for the upper E state [14]; (ii) a comprehensive set of *ab initio* PECs derived in the framework of pure Hund’s coupling cases (a) [9,20] and (c) [21]; (iii) a partial set of *ab initio* spin-allowed transition dipole moments corresponding to pure Hund’s coupling case (a) [20,22]. At the same time transition dipole moments for the required spin-forbidden transitions $E - a; b; c$ [see Fig. 2(b)] are not available yet. It should be noted that, in spite of the considerable progress in *ab initio* calculation of spin-allowed transition dipole moments, the calculations of their spin-forbidden counterparts is still not a straightforward task.

We simulate all relevant spin-allowed and spin-forbidden transition probabilities in order to identify optimal v'_E levels of the E state and to predict the respective laser frequencies for a two-step optical cycle ($X; a$) $^1,3\Sigma^+(v'', J'') \rightarrow E(4)^1\Sigma^+(v'_E, J') \rightarrow X^1\Sigma^+(0,0)$. The efficiency of a two-step optical cycle, in particular of the stimulated Raman transfer, is determined by (i) rovibronic transition probabilities (transition dipole moments) from (to) the ground singlet (triplet) $X; a$ states and the upper E state (see Fig. 1); (ii) radiative properties

of the excited (intermediate) E state, such as radiative lifetimes and electronic branching ratios for spin-allowed [see Fig. 2(a)] and spin-forbidden [see Fig. 2(b)] transitions to the lower-lying states, including both bound-bound and bound-continuum parts of the spectra.

The reliability of modeling will be proved by comparison of calculated transition probabilities with relevant experimental data on relative intensity distributions in the respective $E \rightarrow X$ and $E \rightarrow a$ LIF spectra obtained by high-resolution Fourier-transform (FT) spectroscopy [14,18,19]. The main experimental problem for comparison of LIF intensities in the spectra covering a wide spectral range appeared to be the accurate calibration of the spectral sensitivity of the FT device. Here, calibration of spectral sensitivity has been accomplished by a comparison of experimentally recorded intensity distribution in long LIF progressions of $B^1\Pi_u(v', J') \rightarrow X^1\Sigma_g^+(v'', J'')$ transitions of the K_2 molecule with its theoretical counterparts.

II. TRANSITION PROBABILITIES AND BRANCHING RATIOS

A. Transition probabilities

Total probability P^t of the pump-dump $X; a \rightarrow E \rightarrow X(v=0, J=0)$ optical transfer is proportional to a product of individual probabilities of the stimulated $X; a \rightarrow E$ absorption and $E \rightarrow X$ emission rovibronic transitions:

$$P^t \sim [P_{X;a \rightarrow E}^{v', J' \rightarrow v'', J''=0 \rightarrow v', J'=1}] [P_{E \rightarrow X}^{v', J'=1 \rightarrow v=J=0}]. \quad (1)$$

The required transition probabilities are proportional to a product of the wave number ν_{Ef} of a rovibronic transition $E(v', J') \leftrightarrow f(v'', J'')$, where $f \in X; a$, and the respective squared transition dipole matrix element M_{Ef} :

$$P_{E \leftrightarrow f}^{v', J' \leftrightarrow v'', J''} \sim \nu_{Ef} |M_{Ef}|^2 S^{J' J''}, \quad (2)$$

$$\nu_{Ef}^{v', J' \leftrightarrow v'', J''} = \nu_{E'}^{v', J'} - \nu_f^{v'', J''}, \quad (3)$$

$$M_{Ef}^{v', J' \leftrightarrow v'', J''} = \langle v_E^{J'} | d_{Ef} | v_f^{J''} \rangle, \quad (4)$$

where $S^{J' J''}$ are the Hönl-London factors [23].

In what follows the relevant rovibronic energies E^{vJ} and wave functions $|v^J\rangle$ are obtained by numerical solution of uncoupled radial Schrödinger equation with highly accurate adiabatic empirical potentials available for both ground $X; a$ [18,19] and upper E [14] states, whereas the dipole moment functions $d_{Ef}(R)$ required for the spin-allowed $E - X$ and spin-forbidden $E - a$ transitions are obtained by a quasirelativistic *ab initio* calculations performed in Sec. III.

B. Radiative lifetimes and branching ratios

The radiative lifetime τ_E of the upper E state

$$\frac{1}{\tau_E^{v' J'}} = \sum_f \sum_{v''} \sum_{J''} A_{E \rightarrow f}^{v' J' \rightarrow v'' J''}, \quad (5)$$

and vibronic branching ratios $R_{E \rightarrow f}$ into lower-lying singlet and triplet electronic f states, (where $f \in$

$X; A; C^1\Sigma^+; B^1\Pi; a; c^3\Sigma^+; b^3\Pi$), namely

$$R_{E \rightarrow f}^{v' J'} = \tau_E^{v' J'} \left[\sum_{v''} \sum_{J''} A_{E \rightarrow f}^{v' J' \rightarrow v'' J''} \right], \quad (6)$$

are determined by respective Einstein coefficients of spontaneous emission A_{Ef} [23]:

$$A_{E \rightarrow f}^{v' J' \rightarrow v'' J''} = \frac{8\pi^2}{3\hbar\epsilon_0} \nu_{Ef}^3 |M_{Ef}|^2 S^{J' J''}. \quad (7)$$

A tedious summation over bound and continuum vibrational levels of the lower rovibronic states required in Eq. (5) and (6) is avoided by the approximate sum rule [24,25]:

$$\frac{1}{\tau_E^{v' J'}} \approx \frac{8\pi^2}{3\hbar\epsilon_0} \langle v_E^{J'} | \sum_f \Delta U_{Ef}^3 d_{Ef}^2 | v_E^{J'} \rangle, \quad (8)$$

$$R_{E \rightarrow f}^{v' J'} \approx \frac{\langle v_E^{J'} | \Delta U_{Ef}^3 d_{Ef}^2 | v_E^{J'} \rangle}{\langle v_E^{J'} | \sum_f \Delta U_{Ef}^3 d_{Ef}^2 | v_E^{J'} \rangle}, \quad (9)$$

where $U_{Ef}(R) = U_E(R) - U_f(R)$ are difference potentials. The sums of Franck-Condon factors (FCFs),

$$S_{E \rightarrow f}^{\text{FCF}} = \sum_{v_f=0}^{v_f^{\max}} |\langle v_E^{J'} | v_f^{J'} \rangle|^2, \quad (10)$$

over all bound levels of X and a states, along with vibrational branching ratios

$$\tilde{R}_{E \rightarrow f}^{v' J'} \approx 1 - \frac{\sum_{v_f=0}^{v_f^{\max}} \nu_{Ef}^3 |M_{Ef}|^2}{\langle v_E^{J'} | \Delta U_{Ef}^3 d_{Ef}^2 | v_E^{J'} \rangle}, \quad (11)$$

were estimated as well in order to elucidate the contribution of bound-continuum decay channels into the total probabilities of $E \rightarrow X$ and $E \rightarrow a$ transitions. To test the accuracy of the approximate sum rules (8) and (9), lifetimes and branching ratios have been complementarily calculated by direct summations (5) and (6) for low vibrational levels where the sum over corresponding FCFs is close to 1. The resulting values coincided with their approximate experimental counterparts within 0.01% to 0.05% for several lowest levels with $S_{E \rightarrow X}^{\text{FCF}} \geq 0.9999$.

III. CALCULATION OF TRANSITION DIPOLE MOMENTS

A. Approach

The spin-allowed singlet-singlet $d_{if}^{s-s}(R)$ and triplet-triplet $d_{if}^{t-t}(R)$ transition dipole moments of the KCs molecule were directly evaluated for a wide range of internuclear distance in the basis of the spin-averaged wave functions corresponding to pure Hund's coupling case (a).

For nominally forbidden singlet-triplet $E(4)^1\Sigma^+ - ^3\Sigma^+; ^3\Pi$ transitions the respective effective transition dipole moments $d_{Ef}^{s-t}(R)$ were approximated by a linear combination of the relevant triplet-triplet $d_{if}^{t-t}(R)$ transition dipole moments,

$$d_{Ef}^{s-t} \approx \sum_i c_{Ei} d_{if}^{t-t}, \quad (12)$$

where c_{Ei} are the mixing coefficients between singlet and triplet states, which were determined by construction and

diagonalization of the entire relativistic Hamiltonian including spin-orbit coupling effect: $\mathbf{H}^{(c)} = \mathbf{H}^{(a)} + \mathbf{V}^{so}$, where $\mathbf{H}^{(c)}$, $\mathbf{H}^{(a)}$ are nuclear clamped electronic Hamiltonians corresponding to pure (a) and (c) Hund's coupling cases, respectively. Thus, the eigenvalues of the $\mathbf{H}^{(c)}$ are the adiabatic potential curves given in Ω representation. Hereafter, we assume that the empirical PEC derived for E state in Ref. [14] is identical to the eigenvalue of the relativistic Hamiltonian $\mathbf{H}^{(c)}$.

According to the selection rule $\Delta\Omega = 0$ [23], the $^1\Sigma^+$ state is directly coupled only with the $\Omega = 0^-$ (e symmetry) component of triplet $^3\Pi$ states. Therefore, mixing coefficients c_{Ei} were obtained by using the R -dependent SOC matrix elements V_{Ei}^{so} evaluated between the $E(4)^1\Sigma^+$ and first five low-lying $i \in (1-5)^3\Pi$ states, relevant adiabatic PECs $U_i^{\Omega=0} = U_i^{\Omega=1} - A_i^{so}$ as well as spin-orbit (SO) splitting functions A_i^{so} between the different $\Omega = 0, 1, 2$ components of the $^3\Pi_i^{\Omega}$ states. The second-order SOC effects between the $(4)^1\Sigma^+$ and $^3\Sigma^+$, $^1\Pi$ states manifold were neglected.

B. Computational details

The inner core shells of the K and Cs atoms were replaced with spin-orbit averaged nonempirical effective core potentials (ECPs), leaving nine valence electrons (9 ve) of each atom for explicit treatment. In order to monitor the basis set dependence of the quasirelativistic calculations with respect to both shape [26,27] (ECP1) and energy [28] (ECP2), the consistent small core ECP basis sets of the Cs atom have been used (see Fig. 4). The original shape-consistent ECP1 [29] was augmented by a diffuse part of the all-electron bases for electric property calculation [30] and extended by diffuse and polarization functions [26,27]. The energy-consistent ECP [28] was extended by additional diffuse and polarization functions as well [20]. The relevant spin-averaged and spin-orbit Gaussian basis sets used for each atom were borrowed from the above references. The l -independent core polarization potentials (CPPs) of both atoms were employed together with the above small-core ECPs to take into account for implicitly the residual core-polarization effects [31]. The corresponding ECP scaling SO basis coefficients and CPP cutoff radii were adjusted for each atom in order to reproduce experimental fine-structure splitting of the K($4^2P_{1/2,3/2}$) and Cs($5^2D_{3/2,5/2}$) states [32], respectively.

The optimized molecular orbitals (MOs) were constructed from the solutions of the state-averaged complete active space self-consistent field (SA-CASSCF) problem for 18 electrons. The lowest $(1-4)^1,^3\Sigma^+$ and $(1-5)^1,^3\Pi$ electronic states calculated using the C_{2v} Abelian point subgroup were taken with equal weights [33]. The dynamical correlation effects were introduced by internally contracted multireference configuration interaction (MR-CI) method [34], which was applied for only two valence electrons, keeping the rest frozen, that is, in a full valence (two electrons) CI scheme.

All electronic structure calculations were performed by means of the MOLPRO v.2010.1 program package [35].

C. Transition dipole moment and SOC functions

The resulting spin-allowed $E(4)^1\Sigma^+ - (1-3)^1\Sigma^+$; $(1;2)^1\Pi$ and $(1-5)^3\Pi - a^3\Sigma^+$ transition dipole moments of the KCs molecule are presented in Fig. 3 while the

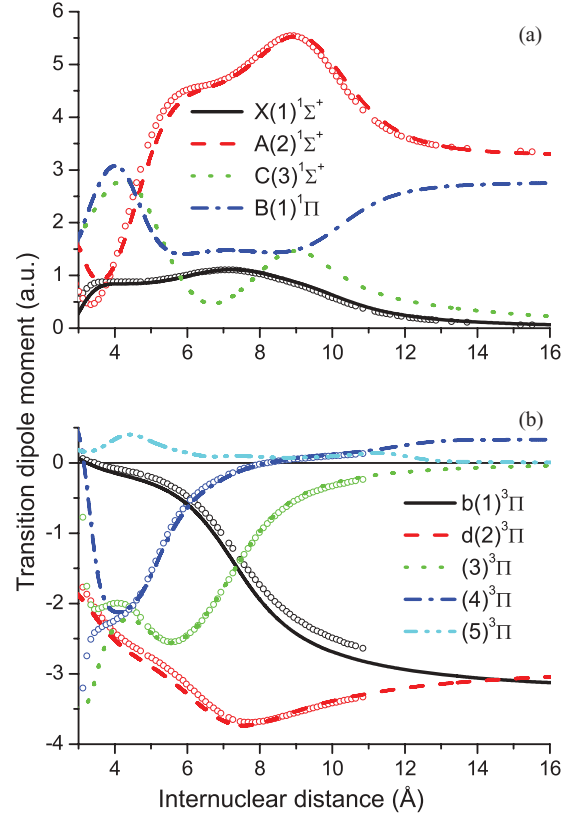


FIG. 3. (Color online) The *ab initio* spin-allowed (a) $d_{E_f}^{s-s}$ singlet-singlet $E(4)^1\Sigma^+ - X, A, C^1\Sigma^+; B^1\Pi$ and (b) $d_{E_f}^{t-t}$ triplet-triplet $(1-5)^3\Pi - a^3\Sigma^+$ transition dipole moment functions. The lines denote the present results while open circles correspond to their preceding counterparts [22].

spin-forbidden $E(4)^1\Sigma^+ - (1;2)^3\Sigma^+; (1)^3\Pi$ transition dipole moments $d_{E_f}^{s-t}(R)$ and respective SOC matrix elements $V_{Ei}^{so}(R)$ between the $E(4)^1\Sigma^+$ and lowest five $^3\Pi$ electronic states are depicted in Fig. 4. The R -dependent mixing coefficients c_{Ei} [where $i \in (1-5)^3\Pi$] derived by a numerical diagonalization of the relativistic Hamiltonian $\mathbf{H}^{(c)}$ agree very well (except at small and large internuclear distances) with those evaluated explicitly in the framework of the nondegenerate perturbation theory, namely $c_{Ei} \approx V_{Ei}^{so}/\Delta U_{Ei}$, where $\Delta U_{Ei}(R)$ is the difference of the corresponding adiabatic PECs. As follows from the energy viewpoint (see Fig. 1), the upper E state is mainly perturbed by the nearby lying $(3)^3\Pi$ state converging to the same dissociation limit $K(4)^2S + Cs(5)^2D$. Nevertheless, the dominating contribution into the spin-forbidden transition dipole moment $E(4)^1\Sigma^+ - a^3\Sigma^+$ [Fig. 4(b)] indeed comes from the lower-lying $d(2)^3\Pi$ state due to the large amplitude of the $d^3\Pi - a^3\Sigma^+$ transition dipole moment [see Fig. 3(b)].

IV. INTENSITY DISTRIBUTION ANALYSIS

A. Approach

To test the reliability of the predicted transition probabilities and corresponding branching ratios, the intensity distributions in the rotationally resolved $E(4)^1\Sigma^+ \rightarrow X^1\Sigma^+$ and $E(4)^1\Sigma^+ \rightarrow a^3\Sigma^+$ spectra $I_{E \rightarrow X;a}^{\text{expt}}$ were measured for several $E(v', J') \rightarrow X; a(v'', J'' = J' \pm 1)$ LIF progressions.

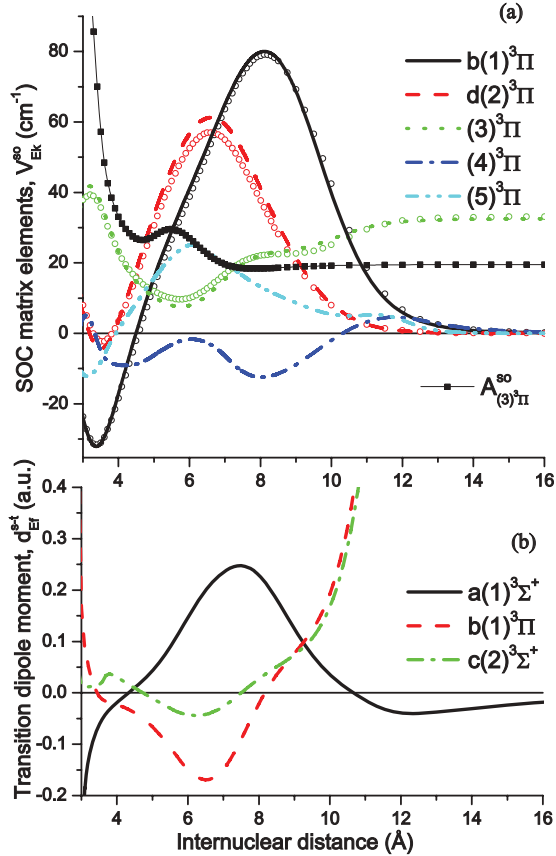


FIG. 4. (Color online) (a) The *ab initio* SO coupling functions $V_{E_i}^{so}$ calculated between the KCs $E(4)^1\Sigma^+$ and $(1-5)^3\Pi$ states as well as the SO splitting function A^{so} for the $(3)^3\Pi$ state. The solid lines and open symbols denote the results corresponding to the shape (ECP1)- and energy (ECP2)-consistent atomic basis sets, respectively. (b) The *ab initio* transition dipole moments $d_{E_f}^{st}$ calculated for the spin-forbidden singlet-triplet $E(4)^1\Sigma^+ - (1; 2)^3\Sigma^+$; $(1)^3\Pi$ transitions.

Then they were compared with their theoretical counterparts

$$I_{E \rightarrow f}^{v'J' \rightarrow v''J''} \sim \nu_{E_f} A_{E \rightarrow f}^{v'J' \rightarrow v''J''}, \quad (13)$$

where $A_{E \rightarrow f}$ is the Einstein coefficient of spontaneous emission defined by Eq. (7). It should be noted that, by using the factor ν in relation (13), it is tacitly assumed that the output signal of a photomultiplier (PM) detector is proportional to the intensity of the incoming fluorescence.

The spectral sensitivity of the recording system was determined in the visible region of the spectra by a comparison of the calculated $K_2 B^1\Pi_u \rightarrow X^1\Sigma_g^+$ rovibronic transition intensities $I_{B \rightarrow X}^{calc}$ with experimental relative intensity distribution $I_{B \rightarrow X}^{expt}$ in the relevant $B \rightarrow X$ LIF spectra. Such an “unconventional” method of calibration possesses the following advantages: (1) the $B - X$ spectra of K_2 and the analyzed $E - a$; X spectra of KCs have the same optical path; (2) the highly accurate adiabatic (nonperturbed) PECs of the $B^1\Pi_u$ and the $X^1\Sigma_g^+$ states of K_2 are available [36,37]; (3) the possible systematic error of an *ab initio* $K_2 B - X$ transition dipole moment is small enough, being comparable with or even less than the experimental uncertainty of the relative intensity measurements.

B. Experiment

The experimental setup was the same as was used in our previous studies [14,18,19].

Briefly, KCs molecules were produced, along with K_2 and Cs_2 molecules, in a linear stainless-steel heat pipe. The heat pipe was filled with 10 g of K (natural isotope mixture) and 7 g of Cs (both metals in ampules from Alfa Aesar). The typical operating pressure of Ar buffer gas was 3–5 mbar. During the experiments the heat pipe was kept at about 290 °C temperature.

The KCs molecules were excited in a transition $E(4)^1\Sigma^+(v', J') \rightarrow X^1\Sigma^+(v'', J'' = J' \pm 1)$ by dye laser radiation at fixed laser frequencies within 16 050 to 17 980 cm⁻¹. The LIF spectra were recorded by FT spectrometer Bruker IFS-125HR at instrumental resolution of 0.03 cm⁻¹.

The LIF spectra were detected in the range from 13 000 to 17 000 cm⁻¹ by a PM operating at room temperature. In order to suppress the He-Ne laser used in the FTS for calibration of the path difference, a notch filter was placed before the detector, thus cutting the spectra in the range from 15 590 to 15 930 cm⁻¹. In order to eliminate the scattered exciting laser light long-pass edge filters were used cutting the high-frequency part of LIF spectra. As a result, the recorded LIF progressions were cut off for low v''_X (see Fig. 5).

Recorded LIF progressions to the ground $X^1\Sigma^+$ state consist of P and R branches. In addition to the dominating spin-allowed $E(4)^1\Sigma^+ \rightarrow X^1\Sigma^+$ transitions, in some spectra we observed weak progressions at a lower frequency range assigned to the spin-forbidden transitions to the ground triplet $a^3\Sigma^+$ state (see also Refs. [18,19]). An example of the observed spectra containing both bands is presented in Fig. 5.

Assignment of the ground-state rotational J'' (N'' in case of $a^3\Sigma^+$) and vibrational v''_X, v''_a quantum numbers for detected progressions, as well as of rotational quantum number J' and the energy of the upper state, was based on the empirical PECs of the ground singlet and triplet states presented in Ref. [18,19]. The upper state vibrational quantum number v'_E was determined using PEC from Ref. [14].

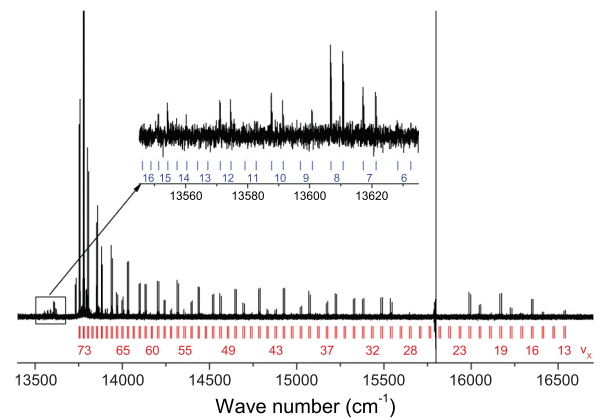


FIG. 5. (Color online) Example of LIF progressions $E(4)^1\Sigma^+ \rightarrow X^1\Sigma^+$ and $E(4)^1\Sigma^+ \rightarrow a^3\Sigma^+$ (see inset) originated from the E state level $v'_E = 25, J'_E = 82$ with energy 17 620.437 cm⁻¹. Spectral lines in wave number range 15 590–15 930 cm⁻¹ are not seen due to the notch filter.

Relative intensity distributions in the $E \rightarrow X, E \rightarrow a$ LIF progressions were determined as follows. Direct readings of the experimental intensities of P and R lines were initially corrected for the small background effect. Then line intensities were corrected according to spectral transmission function of the used long-pass filter FEL610 (from Melles Griot), which was determined from the producer's data sheet. Note that, in case of the $a^3\Sigma^+$ state, each transition to a particular rotational level N'' consists of three well-resolved groups of hyperfine structure (HFS) components. The HFS in the excited state is very small and the excitation from the ground state goes to all excited hyperfine components according to their statistical weight. Hence, the decay back involves similarly all hyperfine components and therefore one can sum over the entire hypermultiplet to obtain the intensity of the transition with no hyperfine splitting. Since in KCs these HFS components almost completely overlap within each group, the intensity of a particular line was determined as a sum of the intensities of all three HFS groups. The measured LIF relative intensities were corrected on the spectral sensitivity of the recording system and normalized on the intensity of the $v'_E \rightarrow v''_{X;a}$ line possessing the maximal intensity in the given progression. Furthermore, the intensities obtained separately for P and R lines were averaged since they appeared to be equal within their uncertainties, as expected for progressions with high J'' . It should be noted, however, that the intensities of P and R lines in some cases can be different for quasibound rovibronic levels. The anomalous intensity ratios of P and R components observed for some R, P doublets seem to be attributed to the influence of a centrifugal barrier on a shape of the respective vibrational wave functions belonging to quasibound levels of the ground $X; a$ states. At the same time, possible interference effects between parallel ($\Delta\Omega = 0$) and perpendicular ($\Delta\Omega = \pm 1$) electronic transitions could be neglected here since the dominant interactions are spin-orbit, for which the selection rule is $\Delta\Omega = 0$.

C. Calibration of spectral sensitivity

The measured intensity distributions in KCs LIF were corrected with respect to the spectral sensitivity $S(\nu)$ of the recording system, including the PM detector and all optical elements. Calibration was performed in the spectral range from 13 500 to 16 500 cm^{-1} by measuring relative intensity distributions in several $\text{K}_2 B^1\Pi_u \rightarrow X^1\Sigma_g^+$ LIF progressions and their comparison with calculated rovibronic transition intensities of the relevant $B - X$ transitions. The spectral sensitivity was defined as

$$S(\nu) = \frac{I_{B \rightarrow X}^{\text{calc}}}{I_{B \rightarrow X}^{\text{expt}}} = a - b \times (\nu - 15000),$$

$$a = 0.826(0.008); \quad b = 1.207(0.102) \times 10^{-4}, \quad (14)$$

where the empirical parameters a and b have been determined by fitting the ratio of the calculated intensities $I_{B \rightarrow X}^{\text{calc}}$ and their experimental counterparts $I_{B \rightarrow X}^{\text{expt}}$. The derived semiempirical function $S(\nu)$ confirms that the sensitivity of recording system gradually increases with ν up to 35%–40% in the spectral range $\nu \in [13\,500, 16\,500] \text{ cm}^{-1}$.

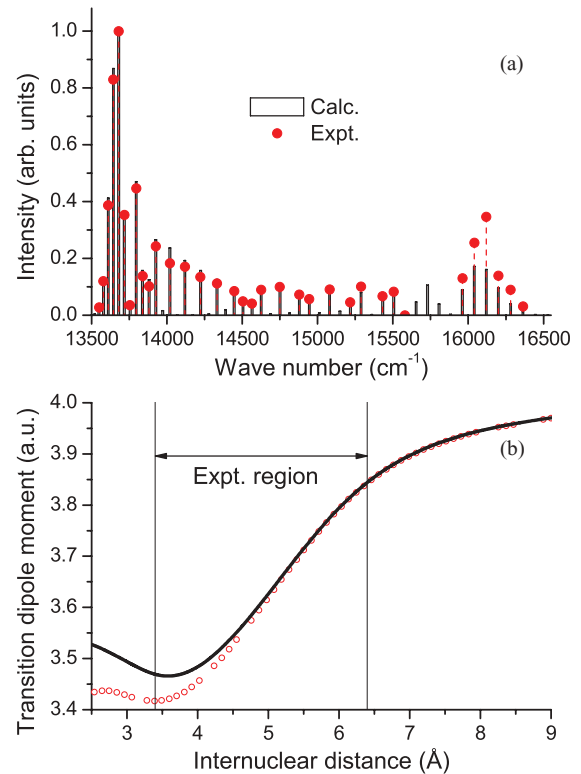


FIG. 6. (Color online) (a) Predicted relative intensity distributions into the $B(v' = 37, J' = 96) \rightarrow X(v''_X)$ LIF progression of $^{39}\text{K}_2$. The absence of the experimental lines in the spectral region around 15 750 cm^{-1} is due to the notch filter. (b) The present (solid line) and preceding (open circles) [22] *ab initio* $B^1\Pi_u - X^1\Sigma_g^+$ transition dipole moments of K_2 . Vertical lines mark the region of R centroids $\langle v'_B | R | v''_X \rangle / \langle v'_B | v''_X \rangle$ corresponding to measured vibronic $v'_B \rightarrow v''_X$ bands.

To perform the intensity measurements, $^{39}\text{K}_2$ molecules were excited in the same heat-pipe using a single-mode dye laser radiation with DCM dye at frequencies 16 197.80 and 16 190.39 cm^{-1} . Here, no filters were used except for the notch filter. The experimental intensities were measured for the four long $B(v', J') \rightarrow X(v'', J'')$ LIF progressions, where (v', J') are (22,25), (27,29), (33,81), and (37,96). Assignment of K_2 progressions was based on molecular constants from Ref. [38]. The comparison of measured and predicted relative intensity distributions in a particular $^{39}\text{K}_2 B(v' = 37, J' = 96) \rightarrow X(v'')$ LIF progression is presented in Fig. 6(a).

The relevant $I_{B \rightarrow X}^{\text{calc}}$ values were estimated by Eq. (13), where the rovibronic energies and eigenfunctions of the upper B and ground X states were obtained from the empirical PEC for the B state [36] and the highly accurate PEC available for the ground X state [37]. The required transition dipole moment $d_{B \rightarrow X}^{\text{K}_2}(r)$ has been calculated according to the same computational scheme as was used for the KCs molecule (Sec. III). The MOs of a homonuclear K_2 dimer were calculated using the D_{2h} subgroup, and the lowest $(1 - 3)^1\Sigma^+$ and $(1 - 2)^1\Sigma^+$ electronic states belonging to both u and g symmetries were simultaneously involved in the SA-CASSCF procedure, yielding the $7\sigma_{u/g}, 8\pi_{u/g}$, and $2\delta_{u/g}$ optimizing MO in an active space. The resulting $\text{K}_2 B^1\Pi_u \rightarrow X^1\Sigma_g^+$ transition dipole moment function depicted in Fig. 6(b) was uniformly

scaled within a few percent to match the empirical atomic transition probability $d_{B-X}^{K_2}(R \rightarrow \infty) = \sqrt{2} \times 2.86$ au on the asymptote $K(4^2P) + K(4^2S)$ [32]. It should be noted that the small divergence observed at small internuclear distance between the present and preceding *ab initio* [22] $K_2 B - X$ transition moment leads to a negligible difference in the respective Einstein coefficients (7) used for spectral sensitivity calibration.

D. Comparison with calculations

The comprehensive comparison of the experimental and calculated relative intensity distributions for a number of LIF progressions has demonstrated their overall agreement, within a few percent for the long $E^1\Sigma^+ \rightarrow X^1\Sigma^+, a^3\Sigma^+$ LIF progressions and within 10%–20% for the respective $I_{E \rightarrow a}/I_{E \rightarrow X}$ vibronic branching ratios. An example of relative intensity distributions obtained for long v'' progressions corresponding to singlet-singlet $E^1\Sigma^+(v'_E) \rightarrow X^1\Sigma^+(v''_X)$ and singlet-triplet $E^1\Sigma^+(v'_E) \rightarrow a^3\Sigma^+(v''_a)$ transitions originating from different E state levels is presented in Fig. 7. As can be seen, the $E \rightarrow X$ measurement covers transitions to $v''_X \in [48; 100]$. Here, the LIF spectrum for lower v''_X values is cut off by a filter in order to improve signal-to-noise ratio for weak transitions to high v''_X levels. In a number of spectra the spin-allowed $E - X$ and spin-forbidden $E - a$ transitions starting from the same upper state level were observed simultaneously. Therefore, the predicted branching ratios

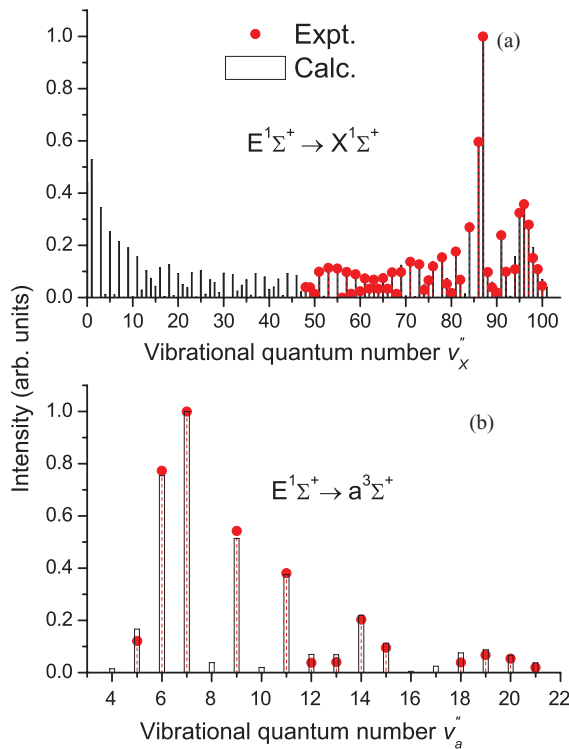


FIG. 7. (Color online) Measured and calculated relative intensity distribution in long LIF progressions corresponding to both spin-allowed $E(4)^1\Sigma^+(v'_E = 45, J' = 21) \rightarrow X^1\Sigma^+(v''_X)$ (a) and spin-forbidden $E(4)^1\Sigma^+(v'_E = 22, J' = 70) \rightarrow a^3\Sigma^+(v''_a)$ transitions (b). Line intensities are normalized to the strongest line in each progression separately.

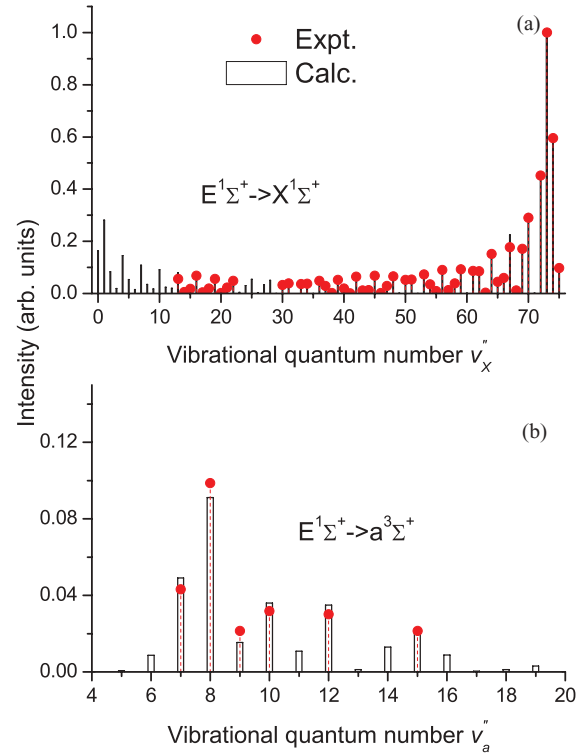


FIG. 8. (Color online) Experimental (see Fig. 5) and calculated LIF intensity distributions in the spin-allowed $E(4)^1\Sigma^+ \rightarrow X^1\Sigma^+$ (a) and spin-forbidden $E(4)^1\Sigma^+ \rightarrow a^3\Sigma^+$ (b) transitions originated from the common level $v'_E = 25, J'_E = 82$. Experimental transitions to $v''_X = 26 \pm 2$ are cut off by a notch filter.

$I_{E \rightarrow a}/I_{E \rightarrow X}$ could be experimentally checked as well. Figure 8 demonstrates consistency of the respective branching ratios $I_{E \rightarrow a}/I_{E \rightarrow X}$ measured and predicted for the spin-allowed $E \rightarrow X$ and spin-forbidden $E \rightarrow a$ transitions, originating from the common $v'_E = 25, J'_E = 82$ level of the E state. The observed agreement of relative intensities and branching ratios supports the correct R behavior of the *ab initio* transition dipole moments as well as the branching ratio of $E \rightarrow X$ and $E \rightarrow a$ transitions. It should be also noted that the reliability of the present spin-allowed transition dipole moments is additionally confirmed by their overall good agreement with their preceding *ab initio* counterparts that are independently derived by the different computational technique [22] [see Figs. 3(a), 3(b), and 6(b)].

V. MODELING OF OPTICAL CYCLE

The present model of the two-step $X^1\Sigma^+, a^3\Sigma^+(v'', J'' = 0) \rightarrow E(4)^1\Sigma^+(v', J' = 1) \rightarrow X^1\Sigma^+(v'' = 0, J'' = 0)$ optical cycle is based on the assumption that translationally and rotationally ($J'' = 0$) ultracold KCs species are initially formed into weakly bound vibrational levels v'' of the ground singlet $X^1\Sigma^+$ and/or triplet $a^3\Sigma^+$ states by PA or MA of ultracold atoms.

The mixing between the ground singlet X and triplet a states (caused by hyperfine Fermi contact interaction) is not taken into account. Such an approximation is apparently not valid for a few highest $X; a$ vibrational levels where the vibrational spacing becomes comparable to the hyperfine splitting. The

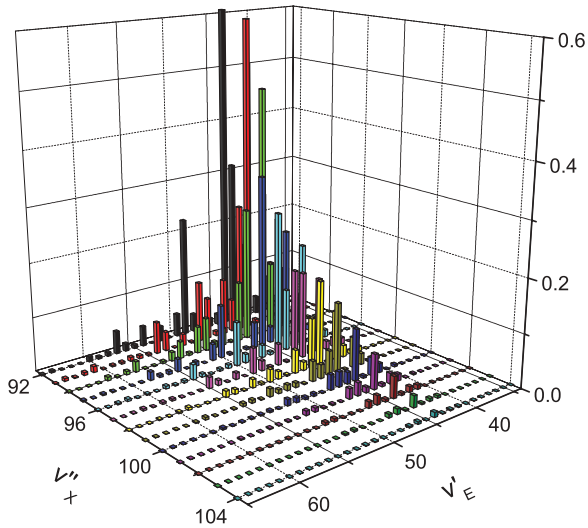


FIG. 9. (Color online) The total probability P^t of the $X(v_X'' \rightarrow E(v_E') \rightarrow X(0,0)$ cycle from high initial vibrational levels v_X'' of the singlet X state. P^t values are normalized to 1 for its largest value at $v_X'' = 90$, $v_E' = 42$, which is not shown in the figure for better visibility of high v_X'' region. The full table is given in Ref. [39].

model also neglects the indirect interactions between the $^1\Sigma^+$ state and F_2 spin-component of $^3\Sigma^+$ states induced by the interference effect between SO and L -uncoupling interaction with high-lying $^1\Pi$ and/or $^3\Pi_0$ states of e symmetry. In contrast to the Fermi contact interaction, this kind of the $X \ ^1\Sigma^+ \sim a \ ^3\Sigma^+$ perturbation could be important only for high rotational levels since the relevant matrix elements are proportional the rotational quantum number $\sqrt{J(J+1)}$.

The individual probabilities $P_{E \leftrightarrow X, a}$ corresponding to both spin-allowed $E(4) \ ^1\Sigma^+(v_E', J_E' = 1) - X \ ^1\Sigma^+(v_X'', J_X'' = 0)$ and spin-forbidden $E(4) \ ^1\Sigma^+(v_E', J_E' = 1) - a \ ^3\Sigma^+(v_a'', J_a'' = 0)$ rovibronic transitions were evaluated according to relation (2) for all bound levels supported by the ground singlet $v_X'' \in [0, 104]$ and triplet $v_a'' \in [0, 32]$ states while the vibrational interval of the intermediate upper E state was restricted by the experimentally observed levels $v_E' \in [0, 75]$ investigated in Ref. [14]. The full tables of results accompanied by the relevant wave numbers of $E - X$ and $E - a$ rovibronic transitions are given in Supplemental Material [39].

The product of resulting transition probabilities P^t calculated by Eq. (1) for the pump-dump $X(v_X'' \rightarrow E(v_E') \rightarrow X(0,0)$ and $a(v_a'' \rightarrow E(v_E') \rightarrow X(0,0)$ optical cycles as dependent on vibrational quantum number of the initial ground v_X'' , v_a'' and intermediate v_E' electronic states are presented in Figs. 9 and 10, respectively.

The total probabilities P^t of the spin-allowed $X \rightarrow E \rightarrow X$ optical cycle are about 20 times larger than their spin-forbidden $a \rightarrow E \rightarrow X$ counterparts. The highest probabilities are expected for the $X \rightarrow E$ and $a \rightarrow E$ pumping transitions starting from well-bound levels of the initial states, namely $v_X'' = 90$ and $v_a'' = 7$, which are not shown in Figs. 9 and 10, but are given in Supplemental Material [39]. However, there are also small but not negligible probabilities to reach the upper E state from weakly bound levels of both X and a states located close to the dissociation limit. In particular, the use of the upper vibrational levels $v_E' = 43, 44$, and 45 should

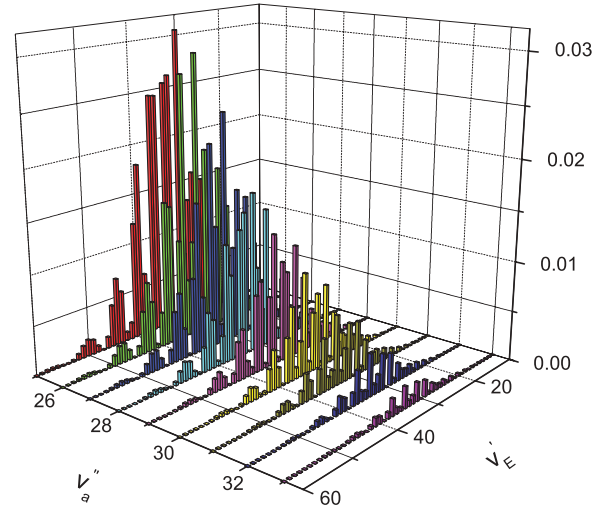


FIG. 10. (Color online) The total probability P^t of the $a(v_a'' \rightarrow E(v_E') \rightarrow X(0,0)$ cycle corresponding to high initial vibrational levels of the triplet a state. The same normalization as in Fig. 9 is preserved. The full table is given in Ref. [39].

provide the feasible excitation from the $v_X'' > 100$ levels of the ground singlet X state. As follows from Fig. 10 there are non-negligible probabilities to excite vibrational levels $v_E' \in [26, 42]$ from the high vibrational levels $v_a'' > 30$ of the triplet a state as well.

It should be noted that our ongoing experiments demonstrate that the $E \rightarrow X$ intensities predicted for the weakly bound $v_X'' \geq 100$ levels slightly overestimate their experimental counterparts. On the contrary, the observed $E \rightarrow a$ intensities for $v_a'' \geq 30$ are significantly larger than their respective adiabatic estimates, presumably because of borrowing probabilities from nearby spin-allowed $E \rightarrow X$ transitions due to pronounced HF mixing between $X \ ^1\Sigma^+$ and $a \ ^3\Sigma^+$ states in the vicinity of dissociation limit. The preliminary coupled-channels calculations [40], which account for HF mixing, qualitatively explain the observed intensity distribution. Thus, the HF mixing (neglected in present calculations) might considerably enlarge the probabilities of $a \rightarrow E$ excitation from the last bound levels of the triplet a state.

Figure 11(a) presents the vibronic branching ratios calculated by Eq. (9) for transitions to the lower-lying singlet X ; A ; B ; C and triplet a states (see Fig. 2). Due to extremely large $E \rightarrow A$ transition dipole moment [see Fig. 3(a)], the spin-allowed $E \rightarrow X$ and $E \rightarrow A$ transitions contribute approximately equal inputs into the total decay of the E state. At the same time, the probabilities of the spin-forbidden $E \rightarrow a$ transitions are about 50–100 times smaller than for the $E \rightarrow X$; A transitions, being comparable with the small branching ratios of the spin-allowed $E \rightarrow B$; C transitions. The contribution of the remaining decay channels could be apparently neglected. Figure 11(b) highlights that the bound-continuum decay channel is negligible for the spin-allowed $E \rightarrow X$ transitions for the $v_E' \lesssim 40$ levels. In contrast, the bound-continuum part of the spin-forbidden $E \rightarrow a$ transition rapidly increases with v_E' and becomes dominant for $v_E' \geq 30$. Thus, bound-continuum transitions are expected to diminish the efficiency of spontaneous emission to the ground $X(0,0)$

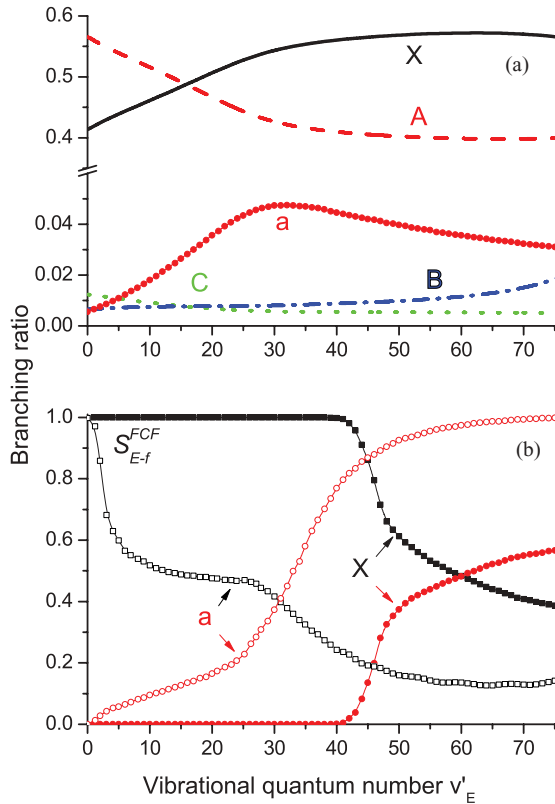


FIG. 11. (Color online) The decay branching ratios of the E state: (a) to the lower-lying singlet X ; A ; $C\ ^1\Sigma^+$, $B\ ^1\Pi$ and triplet $a\ ^3\Sigma^+$ states; (b) to the continuum part of the $E \rightarrow X$ (solid symbols) and $E \rightarrow a$ (open symbols) transitions along with the corresponding sums of Franck-Condon factors $S_{E-X,a}^{FCF}$.

level. In particular, for $v'_E = 44$ about 20% of molecules decay into continuum.

The radiative lifetimes of the intermediate E state were calculated for $v_E, J' = 1$ levels according to the approximate relation (8). The resulting $\tau_E^{v'}$ values monotonically increase with v'_E from 67 to 135 ns for $v'_E \in [0, 75]$.

VI. CONCLUSION

In accordance with the present study, we claim that the translationally ultracold KCs molecules could be efficiently produced in their absolute ground rovibronic state in a two-photon transfer process $X\ ^1\Sigma^+; a\ ^3\Sigma^+(v'') \rightarrow E(4)\ ^1\Sigma^+(v'_E = 44, J'_E = 1) \rightarrow X\ ^1\Sigma^+(0,0)$ from the weakly bound rovibronic levels of the singlet X and triplet a states repopulated by spontaneous decay of the photoassociated laser-cooled atoms or produced by the magnetic Feshbach resonance.

Due to a large probability of undesired bound-bound and bound-free transitions from the $E(4)\ ^1\Sigma^+$ state, implementation of the STIRAP technique is essential.

We believe that the shelflike $E(4)\ ^1\Sigma^+$ state is a promising intermediate state for efficient production of deeply bound ultracold RbCs molecules as well. The modeling of the respective optical cycles in the RbCs molecule is currently in progress.

ACKNOWLEDGMENTS

The authors are indebted to Eberhard Tiemann for numerous helpful discussions and valuable comments on the manuscript, as well as to Olivier Dulieu for providing the nonpublished transition dipole moment data. The support from the Latvian Science Council Grant No. 09.1567 is gratefully acknowledged by I.K., O.N., M.T., and R.F. are indebted to ESF Grant No. 2009/0223/1DP/1.1.1.2.0/09/APIA/VIAA/008. The Moscow team is grateful for support from the Russian Foundation for Basic Researches by Grant No. N10-03-00195-a.

- [1] R. Krems, W. S. Stwalley, and B. Friedrich (eds.), *Cold Molecules: Theory, Experiment, Applications* (Taylor & Francis, Boca Raton, FL, 2009).
- [2] O. Dulieu and C. Cabbanini, *Rep. Prog. Phys.* **72**, 086401 (2009).
- [3] K.-K. Ni, S. Ospelkaus, M. H. G. de Miranda, A. Pe'er, B. Neyenhuis, J. J. Zirbel, S. Kotochigova, P. S. Julienne, D. S. Jin, and J. Ye, *Science* **322**, 231 (2008).
- [4] J. Deiglmayr, A. Grochola, M. Repp, K. Mörtlbauer, C. Glück, J. Lange, O. Dulieu, R. Wester, and M. Weidemüller, *Phys. Rev. Lett.* **101**, 133004 (2008).
- [5] P. Zabawa, A. Wakim, A. Neukirch, C. Haimberger, N. P. Bigelow, A. V. Stolyarov, E. A. Pazyuk, M. Tamanis, and R. Ferber, *Phys. Rev. A* **82**, 040501 (2010).
- [6] J. M. Sage, S. Sainis, T. Bergeman, and D. DeMille, *Phys. Rev. Lett.* **94**, 203001 (2005).
- [7] M. Debatin, T. Takekoshi, R. Rameshan, L. Reichsoelner, F. Ferlaino, R. Grimm, R. Vexiau, N. Bouloufa, O. Dulieu, and H.-C. Nägerl, *Phys. Chem. Chem. Phys.* **13**, 18926 (2011).
- [8] T. Takekoshi, M. Debatin, R. Rameshan, F. Ferlaino, R. Grimm, H.-C. Nägerl, C. R. Le Sueur, J. M. Hutson, P. S. Julienne, S. Kotochigova, and E. Tiemann, *Phys. Rev. A* **85**, 032506 (2012).
- [9] M. Korek, A. R. Allouche, K. Fakherddine, and A. Chaalan, *Can. J. Phys.* **78**, 977 (2000).
- [10] E. R. Hudson, N. B. Gilfoy, S. Kotochigova, J. M. Sage, and D. DeMille, *Phys. Rev. Lett.* **100**, 203201 (2008).
- [11] J.-T. Kim, Y. Lee, B. Kim, D. J. Wang, W. C. Stwalley, P. L. Gould, and E. E. Eyler, *Phys. Rev. A* **84**, 062511 (2011).
- [12] B. Kim and K. Yoshihara, *J. Chem. Phys.* **100**, 1849 (1994).
- [13] A. F. Nogueira, C. E. Fellows, and T. Bergeman, *J. Chem. Phys.* **129**, 136101 (2008).
- [14] L. Busevica, I. Klincare, O. Nikolayeva, M. Tamanis, R. Ferber, V. V. Meshkov, E. A. Pazyuk, and A. V. Stolyarov, *J. Chem. Phys.* **134**, 104307 (2011).
- [15] A. Grochola, J. Szczepkowski, W. Jastrzebski, and P. Kowalczyk, *J. Chem. Phys.* **135**, 044318 (2011).
- [16] O. Docenko, M. Tamanis, J. Zaharova, R. Ferber, A. Pashov, H. Knöckel, and E. Tiemann, *J. Chem. Phys.* **124**, 174310 (2006).
- [17] O. Docenko, M. Tamanis, R. Ferber, H. Knöckel, and E. Tiemann, *Phys. Rev. A* **83**, 052519 (2011).

- [18] R. Ferber, I. Klincare, O. Nikolayeva, M. Tamanis, H. Knöckel, E. Tiemann, and A. Pashov, *J. Chem. Phys.* **128**, 244316 (2008).
- [19] R. Ferber, I. Klincare, O. Nikolayeva, M. Tamanis, H. Knöckel, E. Tiemann, and A. Pashov, *Phys. Rev. A* **80**, 062501 (2009).
- [20] J. T. Kim, Y. Lee, and A. V. Stolyarov, *J. Mol. Spectrosc.* **256**, 57 (2009).
- [21] M. Korek, Y. A. Moghrabi, and A. R. Allouche, *J. Chem. Phys.* **124**, 094309 (2006).
- [22] M. Aymar and O. Dulieu (private communication, 2010).
- [23] H. Lefebvre-Brion and R. W. Field, *The Spectra and Dynamics of Diatomic Molecules* (Academic Press, New York, 2004).
- [24] J. Tellinghuisen and P. S. Julienne, *J. Chem. Phys.* **81**, 5779 (1984).
- [25] A. V. Stolyarov and V. I. Pupyshev, *Phys. Rev. A* **49**, 1693 (1994).
- [26] S. O. Adamson, A. Zaitsevskii, E. A. Pazyuk, A. V. Stolyarov, M. Tamanis, R. Ferber, and R. Cimraglia, *J. Chem. Phys.* **113**, 8589 (2000).
- [27] A. Zaitsevskii, E. A. Pazyuk, A. V. Stolyarov, O. Docenko, I. Klincare, O. Nikolayeva, M. Auzinsh, M. Tamanis, and R. Ferber, *Phys. Rev. A* **71**, 012510 (2005).
- [28] I. S. Lim, P. Schwerdtfeger, B. Metz, and H. Stoll, *J. Chem. Phys.* **122**, 104103 (2005).
- [29] R. B. Ross, J. M. Powers, T. Atashroo, W. C. Ermler, L. A. LaJohn, and P. A. Christiansen, *J. Chem. Phys.* **93**, 6654 (1990).
- [30] A. J. Sadlej and M. Urban, *J. Mol. Struct.: THEOCHEM* **234**, 147 (1991).
- [31] I. S. Lim, W. C. Lee, Y. S. Lee, and G.-H. Jeung, *J. Chem. Phys.* **124**, 234307 (2006).
- [32] NIST Atomic data base, [<http://physics.nist.gov/>].
- [33] H.-J. Werner and P. J. Knowles, *J. Chem. Phys.* **82**, 5053 (1985).
- [34] P. J. Knowles and H.-J. Werner, *Theor. Chim. Acta* **84**, 95 (1992).
- [35] H.-J. Werner *et al.*, MOLPRO, version 2010.1, a package of *ab initio* programs.
- [36] J. Heinze, U. Schöhle, F. Engelke, and C. D. Caldwell, *J. Chem. Phys.* **87**, 45 (1987).
- [37] A. Pashov, P. Popov, H. Knöckel, and E. Tiemann, *Eur. Phys. J. D* **46**, 241 (2008).
- [38] C. Amiot, J. Verges, and C. E. Fellows, *J. Chem. Phys.* **103**, 3350 (1995).
- [39] See Supplemental Material at <http://link.aps.org/supplemental/10.1103/PhysRevA.85.062520> for transition dipole moment functions, SO functions, transition probabilities, and transfer cycle probabilities.
- [40] E. Tiemann (private communication, 2012).